Nuclear Physics B (Proc. Suppl.) 9 (1989) 227–241
North-Holland, Amsterdam

SPECTRUM OF THE PURE GLUE THEORY

Pierre van BAAL

Theory Division, CERN, CH-1211 Geneva 23, Switzerland

Andreas S. KRONFELD

Theoretical Physics Group, Fermi National Accelerator Laboratory,* PO Box 500, Batavia IL 60510, USA

This review is in two parts; it presents the status of the spectrum for the low-lying glueballs and the ('t Hooft) string tension in pure gauge theory. Part I compares numerical simulations of SU(2) lattice gauge theory with analytic (continuum) calculations in intermediate volumes. In particular it deals with the issues surrounding the T_2^+ and E^+ glueballs. It also discusses a new zero-momentum effective Lagrangian, the analytic calculations for asymmetric volumes in relation with the deconfining temperature and the recent results for twisted boundary conditions. Part II outlines problems facing numerical simulations, which had brought progress to a standstill. It reviews methods which are aimed at mitigating these problems. Their implementation has recently yielded a wealth of results that are, by and large, quite consistent. Finally, this part tabulates "world averages" for the scalar and tensor glueballs, as determined in numerical simulations of pure lattice gauge theory.

Part I
COMPARISON OF MONTE CARLO AND ANALYTIC RESULTS FOR SU(2)

1. INTRODUCTION

In Part I of this review we will discuss the comparison between analytic and Monte Carlo results in intermediate volumes for SU(2) gauge theory. Part II will concentrate on the Monte Carlo method, in particular the recent progress for finding operators with a large overlap with the glueball wave functions.

The outline of Part I is as follows. We will first give the Monte Carlo data for SU(2) pure gauge theory obtained since last year's lattice conference at Seillac.[1] Michael, Tickle and Teper[2] found the mass for the T_2^+ glueball in intermediate volumes to disagree with last year's analytic prediction.[3] Vohwinkel[4] showed that this discrepancy could be resolved by a change in associating electric flux quantum numbers to the T_2^+ state. We discuss the present status of these issues. Next we say a few things about an effective Lagrangian used by Kripfganz and Michael[5] to calculate the intermediate volume low-lying spectrum. Then we move on to discuss the analytic calculation of Berg, Vohwinkel and Korthals-Altes[6] in asymmetric boxes, aimed at understanding the deconfining transition. We end Part I with a comparison of preliminary Monte Carlo data by Stephenson and Teper[7] for the spectrum in the presence of twisted boundary conditions, with the recent analytic results of Daniel, Gonzalez-Arroyo, Korthals-Altes and Söderberg.[8]

2. T_2^+ OR NOT T_2^+ AND THE TALE OF THE SPECTRUM

In fig. 1 we collect all lattice Monte Carlo data for the low-lying positive parity states in SU(2), obtained since the lattice conference of Seillac.[1] We plot the mass ratios with the scalar glueball mass $m_{A_1^+}$ as a function of the Lüscher scale parameter[9] $z_{A_1^+} = m_{A_1^+} \cdot L$, where L is the size of the cubic volume. Since the volumes are still finite the cubic symmetry is relevant. We thus classify the states by the irreducible representations of the cubic group, which are tabulated in Part II. It is important to note that all quantities in fig. 1 are dimensionless, which is necessary for comparing results from different regularization schemes. In this way we can compare lattice Monte Carlo and analytic results, based on a continuum calculation in finite volumes.[3]

*Fermilab is operated by Universities Research Association Inc. under contract with the U.S. Department of Energy

0920-5632/89/$03.50

The data originates from the following sources: Michael, Tickle and Teper[2] performed an impressive analysis of *all* representations in both intermediate and large volumes. This breakthrough in scope and extent of the pure glue lattice Monte Carlo analysis is mainly due to the fuzzing procedure, reviewed in Part II, sect. 3. The open circles represent their T_2^+ data, the closed circles the E^+ and the points the $\sqrt{K}$ data (the latter two at the same value of $z_{A_1^+}$ as the T_2^+ data). The finite volume "string tension" K is the energy of 't Hooft's electric flux[10] per unit length. The smallest z ($z = 1.6$) data, as well as the crossed data points, were presented elsewhere[5] as an update of the earlier results.[2] The remainder of the data comes from a universality analysis, using different actions. The squares and triangles are data from Billoire, Decker and Henzi,[11] using a mixed fundamental/adjoint action, whereas the other data (mainly at larger z) originate from Michael and Teper[12] using various actions. (We did not plot the result coming from the fundamental action at $\beta = 2.2$.)

For E^+, A_1^+ and K at intermediate volumes, these data confirm the pioneering results of Berg, Billoire and Vohwinkel.[13,14,15] Fig. 1 also confirms last year's result[16,17,18] that the mass of the E^+ increases by a factor 1.5 when going from $z = 5$ to $z = 10$. We now see that this joins up with the T_2^+ at larger z to form the tensor glueball, apparantly restoring rotational invariance in these larger volumes. Note that within the errors the tensor glueball mass is the multiplicity weighted average mass of the E^+ and T_2^+ states at $z \sim 5$. It is clear, however, that we need better statistics.

We will now discuss the comparison with the analytic results[3,4] indicated in fig. 1 by the solid lines not extending beyond $z \sim 6$, where we expect the approximations to break down.[3,4,19] For $z < 0.8$ we have plotted the perturbative prediction by Lüscher and Münster[20] for E^+ and T_2^+ (which at the scale of fig. 1 are degenerate). It is perhaps worthwhile to say a few words about the region around $z \sim 1$. For $z < 1$ the

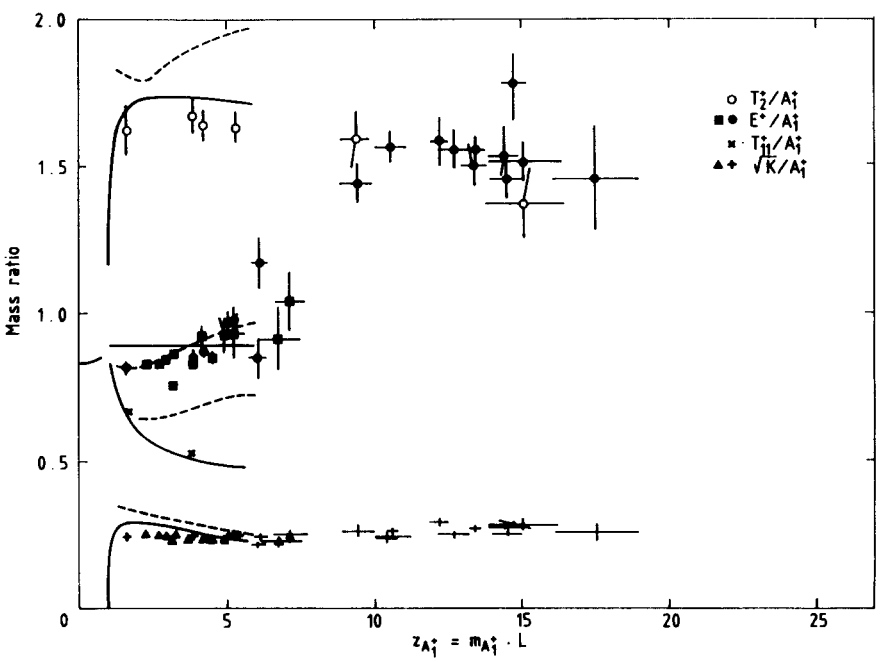

Figure 1: The SU(2) lattice Monte Carlo data[2,11,12] since Seillac for the mass ratios $\sqrt{K}/m_{A_1^+}$, $m_{T_{1_1}^+}/m_{A_1^+}$, $m_{E^+}/m_{A_1^+}$ and $m_{T_2^+}/m_{A_1^+}$ as a function of $z_{A_1^+} = m_{A_1^+} \cdot L$. The solid curves give the analytic predictions[3,4,20] and the dashed curves give the Monte Carlo results obtained from the effective Lagrangian.[5]

electric flux energies go to zero and the nonzero temperature effects, to be discussed in Part II, become important. These effects have been clearly identified by Berg and Billoire[21] and form a technical obstacle for obtaining accurate data in this region. Also in the analytic calculations, based on a Rayleigh-Ritz analysis, one has difficulty in getting accurate results due to the (de-)localization of the wave function, which is why the small and intermediate volume analytic results are not connected by a solid curve. All this intricate dynamics occurs in a very small window of z-values. This is because $z_{A_1^+}$ is almost independent of the physical size L (or equivalently the renormalized coupling constant) over the range where for example the "string tension" K changes from zero to close to its asymptotic value (to be precise, L increases by about six orders of magnitude, going from $z_{A_1^+} = 0.9$ to $z_{A_1^+} = 1.2$).

The glueball state which taught us most this year was the T_2^+ state. In intermediate volumes the Monte Carlo data[2] give a mass of about 1.7 times the scalar glueball mass. This deviates considerably from the prediction[3] $m_{T_2^+}/m_{A_1^+} \sim 0.5$, indicated by the second full curve in fig. 1. This discrepancy was puzzling in the light of the satisfactory agreement for $\sqrt{K}/m_{A_1^+}$ and $m_{E^+}/m_{A_1^+}$. The resolution of this problem was discovered by Vohwinkel,[4] who noticed that the state originally considered as the T_2^+ glueball, actually carried two units of electric flux. The top solid curve gives his result for the genuine T_2^+ glueball and agrees wonderfully well with the Monte Carlo data. Even more convincing are the crosses, representing the data of the "T_2^+" state in the sector of two units of electric flux. They almost perfectly coincide with the old analytic prediction.[3] This state, labelled by T_{11}^+ was measured in the Monte Carlo analysis using appropriate combinations of a Polyakov line in the fundamental representation, winding around the torus in two directions.[2]

We wish to emphasize that these T_2^+ states show a rather unexpected "binding" effect; adding two units of electric flux to the T_2^+ glueball drastically *decreases* its mass. This is, however, strictly a finite volume effect since at large volumes we expect $m_{T_{11}^+} \propto \sqrt{2}KL$, whereas $m_{T_2^+}$ is expected to go to a constant. Hence for some L these two states will cross. For the rather technical details of the appropriate assignment of the electric flux quantum numbers in the analytic calculation we refer to Vohwinkel[4] and to ref. [19], where the negative parity states are also discussed.

Needless to say, it would be very useful if the dynamically most interesting region of $z = 5$ to $z = 10$ were to be probed in more detail in the near future. The payoff will undoubtedly be a better understanding of what makes QCD tick nonperturbatively. Furthermore, who will pick up Berg's challenge[15,22] to find the QCD string by computing the ratios of energies of electric flux? Also very promising are the calculations of the topological susceptibility in intermediate volumes.[23] These should be useful guidance for the analytic attempts along the lines sketched in ref. [3].

3. AN EFFECTIVE LAGRANGIAN

In this section we discuss an effective Lagrangian for the zero-momentum modes, proposed by Kripfganz and Michael.[5] It avoids the explicit use of different coordinate patches in the Hamiltonian formulation by mapping the zero-momentum gauge fields $A_i(\mathbf{x}) = c_i/L = c_i^a \sigma_a/(2L)$ onto SU(2) group valued matrices:

$$U_j = \exp(ic_j)\,. \tag{3.1}$$

In this formulation the coordinate patches are identified by the sign of $\mathrm{Tr}(U_j)$. Since SU(2) is effectively the three-sphere, we can identify these coordinate patches as the various hemispheres.

Let us recall the effective Hamiltonian up to the relevant order

$$H_{eff} = -\frac{1}{2}\left(\frac{1}{g^2} + \alpha_1\right)^{-1} \frac{\partial^2}{\partial {c_i^a}^2} + \frac{1}{4}\left(\frac{1}{g^2} + \alpha_2\right) F_{ij}^a F_{ij}^a + V_\ell(c)\,. \tag{3.2}$$

Here we have put $L = 1$, α_i are small constants, $F_{ij}^a = -\varepsilon_{abd} c_i^b c_j^d$ and $V_\ell(c)$ is the effective potential

$$V_\ell(c) = \frac{4}{\pi^2} \sum_{\mathbf{n}\neq\mathbf{0}} \frac{\sin^2(\mathbf{n}\cdot\mathbf{r}/2)}{(\mathbf{n}^2)^2} - 2|\mathbf{r}|\,, \tag{3.3}$$

with $r_i = \sqrt{c_i^a c_i^a}$. This is the expression in one coordinate patch, defined by $r_i \leq \pi$. Note that $\mathrm{Tr}(U_i) = 0$ at $r_i = \pi$. The other eight coordinate patches are obtained by reflection in the r_i coordinate at $r_i = \pi$.

The effective Lagrangian is now given by

$$\mathcal{L}_{eff} = \mathcal{L}_{kin} + \mathcal{L}_{FF} + \mathcal{L}_V\,, \tag{3.4}$$

where the three terms are to correspond to their counterparts in the effective Hamiltonian. Kripfganz and Michael used the following expressions:[5]

$$\mathcal{L}_{kin} = \left(\frac{1}{g^2} + \alpha_1\right) \sum_i \mathrm{Tr}(\{\dot{U}_i U_i^\dagger\}^2) \,, \qquad (3.5)$$

$$\mathcal{L}_{FF} = -2\left(\frac{1}{g^2} + \alpha_2\right) \sum_{i<j} \left\{ \frac{4}{3}\mathrm{Tr}(U_i U_j U_i^\dagger U_j^\dagger) - \frac{1}{12}\mathrm{Tr}(U_i^2 U_j^2 U_i^{-2} U_j^{-2}) \right\} \,, \qquad (3.6)$$

whereas $\mathcal{L}_V$ is a polynomial in $(\mathrm{Tr}(U_i^n)/2 - 1)$, chosen such as to reproduce V_ℓ as accurately as possible. The kinetic term is simply proportional to the metric of the three-sphere; in ref. [5] a discretized version was used:

$$\mathrm{Tr}(\{\dot{U}_i U_i^\dagger\}^2) = \lim_{\varepsilon \to 0} -2\mathrm{Tr}(U_i(t) U_i^\dagger(t+\varepsilon))/\varepsilon^2 \,. \qquad (3.7)$$

Furthermore $\mathcal{L}_{FF}$ is such that it reproduces the term proportional to $F_{ij}^a F_{ij}^a$ to quartic order in c.

In fig. 1 we indicated by the dashed curves the Monte Carlo results[5] based on $\mathcal{L}_{eff}$ (using the Haar measure in the the path integral). It does describe the main features of the intermediate volume glueball spectrum and in particular also shows that the T_2^+ glueball is about twice as heavy as the scalar glueball. But it deviates, especially at larger z values, considerably from the analytic results. The reason is that the kinetic term should be that of flat three-space, the $O(c^6)$ terms in $\mathcal{L}_{FF}$ are nonnegligible, and $\mathcal{L}_V$ fails to describe V_ℓ accurately around $r_i = \pi$. All these effects become important at larger z values, when the wave function will be probing the region around $r_i = \pi$. As we described in detail elsewhere,[24] all these deficiencies can be easily fixed using a conformal mapping of S^3 to flat three-space, giving:

$$U_j = k_j \cdot \frac{(\pi + i c_j)^2}{\pi^2 + r_j^2} \,, \qquad (3.8)$$

with $k_j = \pm 1$ labelling the different coordinate patches. The following path integral[24] will give the exact equivalence with the effective Hamiltonian:

$$Z = \int \prod_{i=1}^{3} \frac{dU_i}{K_i^3} \exp\left(- \int dt \left[\frac{\mathcal{L}_{kin}}{K_i^2} + \hat{\mathcal{L}}_{FF} + V_\ell(\mathbf{r}) \right] \right) \,, \qquad (3.9)$$

where dU_i is the Haar measure,

$$K_i = (2 + |\mathrm{Tr}(U_i)|)/\pi \,, \qquad (3.10)$$

$$\hat{\mathcal{L}}_{FF} = \left(\frac{1}{g^2} + \alpha_2\right) \sum_{i,j} \frac{\mathrm{Tr}(U_i U_j U_i^\dagger U_j^\dagger) - 2}{K_i^2 K_j^2} \,, \qquad (3.11)$$

and

$$r_i = \pi\sqrt{2 - |\mathrm{Tr}(U_i)|}/\sqrt{2 + |\mathrm{Tr}(U_i)|} \,. \qquad (3.12)$$

The advantage of using the SU(2) group variables is that the boundary conditions, which had to be imposed in the Hamiltonian approach, are already properly incorporated. In technical terms they amount to the continuity of the wave function in the vacuum-valley coordinates r_i, but no further analysis is necessary to derive boundary conditions at $r_i = \pi$. In the Lagrangian formulation the appropriate state is selected by using operators with the right quantum numbers. A further advantage is that only a minor modification of the effective Lagrangian will allow one to include massless fermions[5,24] and obtain intermediate volume results for the glueball masses for an arbitrary number of quark flavours, thus extending earlier small volume perturbative calculations.[25] A preliminary conclusion is that at least for SU(2) the mass ratios are rather insensitive to the number of flavours.

4. THE ASYMMETRIC BOX AND Θ_c

In this section we wish to outline the results of Berg, Vohwinkel and Korthals-Altes[6] on the spectrum in an asymmetric box. That is, the gauge fields now satisfy

$$\mathbf{A}(\mathbf{x} + \mathbf{f} \cdot \mathbf{n} L) = \mathbf{A}(\mathbf{x}) \,, \qquad (4.1)$$

with $\mathbf{f}$ describing the asymmetry. Typically we will be interested in the case $f_{ij} = 0$ for $i \neq j$ and

$$f_{11} = 1/z_\Theta \,, \quad f_{22} = f_{33} = 1 \,, \qquad (4.2)$$

with z_Θ the asymmetry parameter considered in ref. [6]. The geometry in the four-dimensional context is that of a hypercube $L_\Theta \times L^2 \times \infty$, with $L_\Theta = L/z_\Theta$. The fourth direction has an infinite extension, since the Hamiltonian formulation will give us zero temperature results. However, if we calculate, say, the energy of electric flux in the L_Θ direction and apply 't Hooft's duality transformation[10] (interchanging the L_Θ and time direction), then we would be calculating a quantity relevant to finite temperature gauge theory.

One can easily calculate the effective Hamiltonian in the small volume perturbation theory (z_Θ fixed, L and L_Θ small), first calculating the effective Lagrangian with the background field method[3] in terms of the zero-momentum gauge fields $A_i = c_i/L$ and then converting back to the Hamiltonian. The result is:

$$L_\Theta \cdot H_{eff}(z_\Theta) = -\frac{1}{2}\left[\frac{1}{g^2(L_\Theta)} + \alpha_1^{(i)}(z_\Theta)\right]^{-1} \frac{\partial^2}{\partial {c_i^a}^2} + \frac{1}{4z_\Theta^2}\left[\frac{1}{g^2(L_\Theta)} + \alpha_2^{(ij)}(z_\Theta)\right] F_{ij}^a F_{ij}^a + V_\ell(c; z_\Theta) \ . \quad (4.3)$$

This clearly reduces for $z_\Theta = 1$ to eq. (3.2), in which case $\alpha_1^{(i)}$ and $\alpha_2^{(ij)}$ are independent of i and j, due to the cubic symmetry. (Here and in eq. (3.2) we neglected terms to $O(c^6)$, which vanish for $F_{ij} = 0$; they, as well as the *small* constants $\alpha_1^{(i)}$ and $\alpha_2^{(ij)}$, have been computed for arbitrary z_Θ in ref. [6].) Furthermore, $V_\ell(c; z_\Theta)$ can be shown to be of the form:

$$V_\ell(c; z_\Theta) = \frac{4}{(\pi z_\Theta)^2} \sum_{\mathbf{n}\neq 0} \frac{\sin^2(\mathbf{n}\cdot\mathbf{r}/2)}{((\mathbf{f}\cdot\mathbf{n})^2)^2} - 2\frac{\sqrt{\sum_{i,a} c_i^a c_i^a}}{z_\Theta} \ , \quad (4.4)$$

where c_i^a is given in terms of the radial coordinates (r_i, θ_i, ϕ_i) by:

$$(c_i^1, c_i^2, c_i^3) = r_i(\cos\phi_i \cos\theta_i, \sin\phi_i \cos\theta_i, \sin\theta_i)/f_{ii} \quad (4.5)$$

These radial parameters play exactly the same role as for $z_\Theta = 1$, in particular they parametrize the basic coordinate patch by $r_i \leq \pi$. Also the complete and gauge invariant basis of wave functions to be used is *exactly* the same as for $z_\Theta = 1$, with the same choice of boundary conditions at $r_i = \pi$.

This was used by Berg, Vohwinkel and Korthals-Altes[6] to calculate for various values of $z_\Theta > 1$ the energy of electric flux ($E(g, z_\Theta)$) as a function of g, where g in this case is the renormalized coupling constant in the minimal subtraction scheme at the scale $\mu = 1/L_\Theta = \Theta$. In the sense explained above, Θ is the physical temperature. Their results clearly indicate that $z_\Theta E(g, z_\Theta)$ tends to a step function in the limit $z_\Theta \to \infty$, with $z_\Theta E(g, z_\Theta) = 0$ for $g < g_c$ and $z_\Theta E(g, z_\Theta) = \infty$ for $g > g_c$. Furthermore, there seems to be a fixed point at g_c with a finite value for $\lim_{z_\Theta\to\infty} z_\Theta E(g_c, z_\Theta)$.

The mass gap in the two-dimensional Ising model shows exactly the same behaviour and the interpretation is therefore that Θ_c, obtained from solving the equation $g(\Theta_c) = g_c$, corresponds to the deconfining temperature. We refer to Berg's contribution to this conference for a further discussion of the results. Despite the inevitable breakdown of the method for z_Θ too large and the fact that higher loop corrections to the two-loop β-function might be nonnegligible at $g_c \sim 2.25$, the results look very convincing and nicely show the interpolation between the tunnelling transition at $z_\Theta = 1$ (around g is 0.7) and the deconfining transition at $z_\Theta = \infty$.[15,26]

5. LET'S TWIST AGAIN

In this section we will describe the use of twisted boundary conditions,[10] causing the presence of magnetic flux. The main motivation for studying twisted boundary conditions is that the classical vacua are isolated due to the twist-induced absence of zero momentum modes, making perturbative calculations much easier.[27,28] The finite volume behaviour is possibly smoother for some quantities,[28] however, for electric flux energies a strong volume dependence (probably around 0.7 fm) is unavoidable.[29] Nevertheless, in sufficiently large volumes one does not expect to observe any dependence on the boundary conditions;[10] the large volume expansion for the glueball masses[30] and the string tension[31] will be independent of the magnetic flux (to the order presently known). But since 1 fm is exactly the distance scale at which confining effects are expected to set in, the use of twisted boundary conditions will be an indispensable additional probe for the physics at this scale.

We will formulate the continuum theory in the Hamiltonian approach in a cubic volume of size L with the following boundary conditions for the gauge fields:

$$\mathbf{A}(\mathbf{x} + L\mathbf{e}_k) = \Omega_k \mathbf{A}(\mathbf{x}) \Omega_k^\dagger \ . \quad (5.1)$$

We have chosen a gauge in which the gauge functions Ω_k are constant SU(N) matrices. They satisfy 't Hooft's consistency conditions, which also give the relation to the magnetic flux $\mathbf{m} \in \mathbb{Z}_N^3$

$$\Omega_k \Omega_\ell \Omega_k^\dagger \Omega_\ell^\dagger = \exp(2\pi i \varepsilon_{k\ell j} m_j / N) \ . \quad (5.2)$$

From now on we only consider SU(2) with $\mathbf{m} = (1, 1, 1)$ realized by

$$\Omega_k = i\sigma_k \ . \quad (5.3)$$

Generalizations to SU(3) (or arbitrary SU(N)) and magnetic flux are easy to obtain.[8] However, the present choice has the additional advantage of not breaking the cubic group ($1 = -1 \mathrm{mod} 2$). Consequently, glueball states are still classified by the irreducible representations of the cubic group.

In lattice gauge theory one can similarly impose twisted boundary conditions on the link variables[32]

$$U_{\ell,\mathbf{n}+N_S\mathbf{e}_k} = \Omega_k U_{\ell,\mathbf{n}} \Omega_k^\dagger \quad (5.4)$$

and to make contact with the Hamiltonian formalism one should choose a time-asymmetric lattice of size $N_T \times N_S^3$, with $N_T \gg N_S$ (in the above equation we sup-

pressed the dependence on the time parameter). The boundary condition in the time direction should be chosen periodic and glueball masses are again measured with adjoint Polyakov loops, whereas electric flux energies are measured with fundamental Polyakov loops, just as in the case of periodic boundary conditions.[13,14] However, in order to preserve the gauge invariance, the definition of the Polyakov loop has to be slightly modified:[33]

$$\mathrm{Tr}\left[P\exp(i\int_0^L A_j(\mathbf{x}+s\mathbf{e}_j)ds)\Omega_j\right] , \qquad (5.5)$$

with a similar definition on the lattice.

It is not too hard to see that the boundary conditions can be solved by the following Fourier expansion:[8,29]

$$\mathbf{A}^a(\mathbf{x}) = \sum_{\mathbf{k}\in\mathbb{Z}^3} \mathbf{A}^a(\mathbf{k}+\mathbf{r}_a)\exp(2\pi i(\mathbf{k}+\mathbf{r}_a)\cdot\mathbf{x}/L) , \qquad (5.6)$$

with

$$\mathbf{r}_a = (\mathbf{e}_a\times\mathbf{m})/2 . \qquad (5.7)$$

Next one uses the Coulomb gauge $\partial_i A_i = 0$ and expands around the classical vacuum $\mathbf{A}=0$, which in this case is isolated with all fluctuations quadratic. There is a discrete subgroup of the gauge transformations:

$$\mathcal{K} = \{1, i\sigma_1, i\sigma_2, i\sigma_3\}\times\{1,-1\} , \qquad (5.8)$$

which leaves the gauge and boundary conditions invariant. The wave functionals are therefore representations of $\mathcal{K}$, and the nontrivial representations carry electric flux as defined by 't Hooft.[10] Obviously, the one-particle states associated with the creation operator $b^\dagger(a,\mathbf{p},\pm)$ belonging to the Fourier mode $\mathbf{A}^a_\pm(\mathbf{p})$ have nonzero electric flux (here $\pm$ stands for the polarization of the gauge field, satisfying $\mathbf{A}^a_\pm(\mathbf{p})\cdot\mathbf{p}=0$). Actually, it is not hard to show that the electric flux vector associated to this state is $\mathbf{e}_a$. This is why one can think of $2\pi\mathbf{r}_a/L$ as a Poynting vector $\mathbf{P}$ (see ref. [8] for details).

Hence, if we are interested in the zero electric flux sector, one needs two-particle states, built from two states with opposite (which for SU(2) is equivalent with identical) electric flux and are thus of the form:

$$b^\dagger(a,\mathbf{p},\varepsilon)b^\dagger(a,\mathbf{q},\delta)|0\rangle , \qquad (5.9)$$

with $\varepsilon,\delta=\pm$ the polarizations of the one-particle states. These states have total momentum $\mathbf{Q}$ and energy E satisfying:

$$\mathbf{Q} = 2\pi(\mathbf{p}+\mathbf{q})/L , \quad E = 2\pi(|\mathbf{p}|+|\mathbf{q}|)/L . \qquad (5.10)$$

Since the smallest value of $|\mathbf{p}|$ is $|\mathbf{r}_a| = \sqrt{2}/2$, the mass gap in lowest order is

$$m_{gap} = 2\pi|\mathbf{e}_a\times\mathbf{m}|/L = 2\pi\sqrt{2}/L , \qquad (5.11)$$

which is twice the length of the Poynting vector. This Poynting vector also plays an interesting role in how the wave functional behaves under translations over L in the three coordinate directions. From very general arguments one finds:[33]

$$|\Psi(\mathbf{x}+L\mathbf{n})\rangle = \exp(i\mathbf{n}\cdot\mathbf{P}L)|\Psi(\mathbf{x})\rangle , \qquad (5.12)$$

with $\mathbf{P}=\pi(\mathbf{e}\times\mathbf{m})/L$ the Poynting vector if $|\Psi\rangle$ has magnetic flux $\mathbf{m}$ and electric flux $\mathbf{e}$.

Since the two-particle states are in many respects very similar to two-photon states, with three coloured species, one easily shows (taking Bose statistics into account) that the colourless, zero momentum, first excited state is 24-fold degenerate. Let us point out that there are nonzero momentum states, which are degenerate with this, thus making the projection of the operators on the zero-momentum sector in a lattice Monte Carlo analysis mandatory. In ref. [8] it is shown that the 24-fold degeneracy will in lowest order split according to the irreducible representations r of the cubic group, leaving a few accidental degeneracies between even/odd parity pairs, which will be lifted in higher order. To lowest order the masses of these various states are given by the parameter γ_R:

$$z_r = m_r\cdot L = 2\sqrt{2}\pi + \frac{g^2(L)\gamma_r}{12\pi^2} , \qquad (5.13)$$

where $g(L)$ is the renormalized coupling constant, obtained by dimensional reduction with minimal subtraction at the scale $\mu = 1/L$. The constants[8] γ_r are given in Table 1.

In fig. 2 we compare the analytic results with recent (preliminary) lattice Monte Carlo data from Stephenson and Teper,[7] for $m_{A_1^+}$, m_{E^+} and $m_{T_2^+}$ at $\beta=2.3$ and $N_T\times N_S^3 = 16\times 4^3$. As one can see, they agree rather well. Stephenson and Teper are working on getting better statistics, going to smaller volumes and calculating electric flux energies, whereas loop corrections for the analytic calculations are underway, which will give us an idea of the range of validity of the first order result.

Table 1: The constants γ_r as they appear in Madrid preprint[8] FTUAM/89-01, January 1989. These differ from what was presented at the conference, but fig.2 remains correct. Note the near even/odd degeneracies.

irrep r	γ_r	#
A_1^+, A_1^-	-69.06,-68.94	2
T_2^+	-30.93	3
E^+	-17.00	2
T_2^+, T_2^-	-5.56,-4.94	6
T_2^+	5.14	3
T_1^+	11.06	3
A_1^+	19.18	1
E^+, E^-	27.12,27.06	4

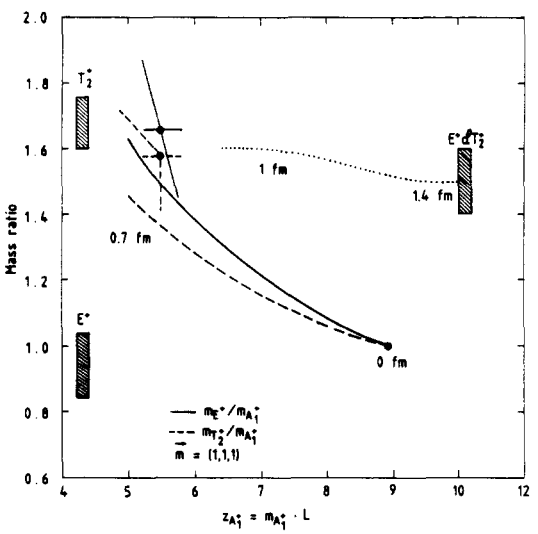

Figure 2: Comparison between lattice Monte Carlo[7] and analytic[8] results for SU(2) with twisted boundary conditions. The dotted curve indicates the anticipated large volume behaviour. We indicated the approximate corresponding values of L. The shaded boxes give the intermediate and large volume results of fig. 1 as a comparison.

Let us end this section with a few words on how to interpret fig. 2. First, the behaviour of $z_{A_1^+}$ as a function of L is distictly different from the case with no twist. In perturbation theory it is a *decreasing* function of L, but it can do so only for small volumes, because at larger volumes the scalar glueball mass will rapidly tend to a constant making $z_{A_1^+}$ grow linearly with L. Hence, at some point the curves for the mass ratios will fold over, presumably around $z_{A_1^+} = 5$. The dotted curve gives the anticipated behaviour at larger volumes, merging with the large volume results obtained in the untwisted case (indicated by the shaded box, labelled $E^+ \& T_2^+$). At various points along the curves we have indicated the approximate corresponding value of L. Second, the T_2^+ and E^+ states never split in intermediate volumes as much as they did in the periodic case. Thus indeed $m_{T_2^+}/m_{E^+}$ is one example of a quantity with a small volume dependence in the twisted case, but e.g. $m_{T_2^+}/m_{A_1^+}$ has a volume dependence comparable to that in the periodic case. In fig. 2 we have also indicated by the shaded boxes around $z = 4$, the result for T_2^+ and E^+ in the case of periodic boundary conditions. Third, as we emphasized before,[29] studying various electric flux energies will give us some interesting clues on the dynamics of the confining region.

6. CONCLUSION

Looking back at the last two years one has to conclude that we have gained a lot of understanding on the dynamics of pure gauge theories. The impressive progress in the lattice Monte Carlo calculations is starting to give us, even in large volumes, a clear picture of the spectrum. It should be a "piece of cake" to fill in the conspicuous gap around $z \sim 7$ in fig. 1. It is also gratifying to see that results with twisted boundary conditions are becoming available. We would like to urge that all these tools be used for probing the intricate dynamics at the scale of 1 fm, where confining effects are expected to set in. From the analytic point there is the challenge to go to larger volumes, for which we believe it is necessary to include instantons and θ dependence.

Part II
NUMERICAL PROGRESS TOWARDS THE CONTINUUM AND LARGE VOLUME LIMITS

1. INTRODUCTION

At present, analytical methods are not reliable for $z \gtrsim 6$, so one still needs numerical simulations to probe the $z \to \infty$ limit. The progress made towards infinite z is the subject of this part of the review. Since the numerical simulation always has a nonzero lattice spacing a, this part of the review also details the progress made in reaching the limit $a \to 0$. In practice, the zero-lattice-spacing limit has been the more daunting problem, but methods have been devised, by a number of groups, to cope with this problem. Efficient numerical methods for large volumes also work well in small volumes, so this discussion is also relevant to the Monte Carlo simulations in the $0 < z \leq 5$ region, covered in Part I.

The presentation is as follows: After some preliminaries on notation (sect. 2), the theoretical framework for extracting the spectrum from a finite lattice is reviewed in sect. 3. Sect. 3 also discusses the origin of noise at finite statistics, the problems of poor signal-to-noise ratios in old-fashioned methods, and the new methods devised to cope with these problems. Readers who are more interested in results than methods will find this section painfully boring, but they are urged to suffer slightly and to skim (at least) the explanation of the problems. Otherwise, the danger of misinterpreting the results is very large! A summary of these results appears in sect. 4, followed by some remarks on future prospects (sect. 5).

2. NOTATION

The simulations are performed on $N_S^3 \times N_T$ hypercubic lattices with lattice spacing a. In all cases (reviewed here) periodic boundary conditions are imposed —spacetime is a torus. In physical units, the linear size of the spatial volume is $L = N_S a$, and the maximum time extent is $T = N_T a$. The fact that N_T is always finite, in practice, implies that the system is at a nonzero physical temperature $\Theta = 1/(N_T a) = 1/T$. The infinite-volume, continuum limit is $a \to 0$ with L fixed, followed by $L \to \infty$. In numerical simulations these limits are "attained" by looking for asymptotic behaviour in the a-dependence at fixed L and in the L-dependence at fixed a.

For all a and L the *transfer matrix* $\hat{T}$ is well-defined: it is the operator which time-translates a (three-dimensional) configuration by one timeslice. Physical states are eigenstates of $\hat{T}$:

$$\hat{T}|n,r\rangle = \mathcal{T}_{n,r}|n,r\rangle, \tag{2.1}$$

where $\mathcal{T}_{n,r}$ is the eigenvalue of $\hat{T}$. The eigenvalue offers a definition of the energy for arbitrary a and L:

$$m_{n,r}(a,L) = a^{-1} \log \mathcal{T}_{n,r}, \tag{2.2}$$

adopting the convention of expressing spectral quantities in physical units. The quantum number n distinguishes excited states within the representation r of the symmetry group for the transfer matrix—or, equivalently, the Hamiltonian. For SU(N) gauge theory, this group is

$$G = \mathbb{Z}_N^3 \cdot S(\mathrm{T}^3) \tag{2.3}$$

where $S(\mathrm{T}^3)$ is the symmetry group of the (continuous or discrete, as appropriate) 3-torus. The center symmetry $\mathbb{Z}_N^3$ is associated with the 't Hooft electric-flux sector.[20] For $N \geq 3$ there is also charge conjugation.

Saturday morning is the *wrong* time to discuss group theory, so we shall focus on only a few representations. In the zero electric-flux sector, i.e. the glueball sector, we shall concentrate on zero 3-momentum, and for the nonzero electric-flux sectors we shall concentrate on the splitting of these sectors' ground states from the ground state of the zero electric-flux sector. These splittings are usually referred to as energies of units of 't Hooft electric flux[3] or as a "torelon mass."[34] In particular, the energy E_1 of the one electric-flux sector is related to the string tension K by[10]

$$K = \lim_{L\to\infty} \frac{E_1}{L}. \tag{2.4}$$

It is common to refer to E_1/L as the ('t Hooft) string tension, even though the interpretation is only clear-cut for large L.

For finite L and nonzero a the rotation group is broken to the symmetry group of a cube—this is then the relevant symmetry group for the (zero-momentum) glueball states. Table 2 lists the irreducible representations, along with their dimensions and the lowest-spin representation of the full rotation group. Especially important to the large z limit are the E and T_2 representations; these states combine to form the tensor ($J = 2$) glueballs. As we have learned from Part I, the E–T_2

Table 2: Irreducible representations of the cubic group.

irrep r	dim	spin J
A_1	1	0
A_2	1	3
E	2	2
T_1	3	1
T_2	3	2

mass difference is rather large for $z \lesssim 5$, whereas for sufficiently large values of z, where rotational invariance ought to be restored, the two states should be degenerate. Consequently, one should stress the distinction between the two states, until Monte Carlo results indicate that they are degenerate, in which case the term "tensor glueball" is justified.

Numerical simulations only determine dimensionless combinations like $am_{n,r}$ or a^2K. The lattice spacing is varied indirectly by adjusting the bare gauge coupling β. As we've seen already in Part I, it is convenient to form dimensionless quantities in which a does not appear. These include mass ratios and $\sqrt{K}/m$, as well as the scaling variable $z_r = N_S a m_{1,r} = L m_{1,r}$, which is the size of the spatial volume in glueball Compton wavelengths. The discussion of the numerical results, sect. 4, focuses on $z = z_{A_1}$, corresponding to the lowest scalar glueball. In terms of these combinations, the infinite-volume, continuum limit has been reached when *all* of these ratios are independent of β and N_S.

3. METHODOLOGY

3.1. Transfer matrix and correlation functions

The masses are determined from correlation functions

$$C_r(t) = \langle : \Phi_r^*(t) : : \Phi_r(0) : \rangle, \tag{3.1}$$

where Φ_r is a function of the lattice gauge field with support on the timeslice n_t: $t = n_t a$. Under the symmetry group of the transfer matrix, the Φ_r transform as an r-tensor. The colons indicate that the vacuum expectation value has been subtracted out, i.e. $C_r(t)$ is a connected correlation function.

In the transfer matrix formulation the correlation function is

$$C_r(t) = \frac{\mathrm{Tr}[\hat{T}^{N_T - n_t} : \hat{\Phi}_r^* : \hat{T}^{n_t} : \hat{\Phi}_r :]}{\mathrm{Tr}[\hat{T}^{N_T}]}, \tag{3.2}$$

where the trace Tr is taken over all physical states, e.g. over all eigenstates of $\hat{T}$. By inserting complete, orthonormal sets of states, one can show that

$$\begin{aligned} C_r(t) = \frac{1}{Z} \Bigg[& \sum_n \left| \langle 0 | : \hat{\Phi}_r : | n, r \rangle \right|^2 \times \\ & \{ \exp(-m_{n,r} t) + \exp[-m_{n,r}(T-t)] \} \\ & + \sum_{l,p} \left| \langle l, p | : \hat{\Phi}_r : | l, p \rangle \right|^2 \exp(-m_{l,p} T) \\ & + \sum_{(l,p) \neq (n,q)} \left| \langle n, q | : \hat{\Phi}_r : | l, p \rangle \right|^2 \times \\ & \exp[-(m_{l,p} - m_{n,q}) t] \exp(-m_{n,q} T) \Bigg], \end{aligned} \tag{3.3}$$

where

$$Z = 1 + \sum_{(n,r) \neq 0} \exp(-m_{n,r} T), \tag{3.4}$$

and $|0\rangle$ denotes the vacuum. Eq. (3.3) is obviously a mess, and part of the art of numerical simulations is choosing the parameters so that it is possible to extract useful information from it. Usually one assumes that $mT \gg 1$ and neglects all but the first sum in eq. (3.3). However, it is important to realize that all states contribute to the second sum, unless they are forbidden by the Wigner-Eckhart theorem. If some state has a very small energy, then T must be huge to suppress this contribution. Relevant examples include the electric flux energy in a small volume[21] and (approximate) Goldstone bosons. Neglecting this term can hamper attempts to extract masses of heavier states from the t-decay of the correlation function.

If T is sufficiently large, the first term in eq. (3.3) dominates. Then for t and $T - t \gg m_{2,r}^{-1}$ we obtain

$$C(t) = A \cosh[m_{1,r}(t - \tfrac{1}{2}T)] + B, \tag{3.5}$$

with

$$A = \frac{1}{Z} \left| \langle 0 | : \hat{\Phi}_r : | 1, r \rangle \right|^2 \exp(-\tfrac{1}{2} m_{1,r} T). \tag{3.6}$$

The mass $m_{1,r}$, and possibly the constant B, which compensates for the nonzero temperature effects, are then determined from a fit to eq. (3.5). Two state fits are also possible.

The method outlined above is called the "correlation method." Another method is the "source method," which introduces a source into the partition function at $t = 0$. The resulting correlation function is then

$$S_r(t) = \frac{\mathrm{Tr}[\hat{T}^{N_T-n_t} : \hat{\Phi}_r^* : \hat{T}^{n_t}\hat{\Psi}]}{\mathrm{Tr}[\hat{T}^{N_T}\hat{\Psi}]}, \qquad (3.7)$$

where Ψ denotes the source. $S_r(t)$ has an expansion similar to eq. (3.3), but the coefficients in the sums are no longer positive definite. To analyze all quantum numbers during one simulation, Ψ must be in a reducible represantation, containing all irreducible representations of interest. A popular choice is the "cold wall," which freezes a two-dimensional plane of links to the unit element.

3.2. Finite statistics, fluctuations, and error bars

A Monte Carlo simulation never reaches infinite statistics. For fixed statistics, the statistical errors are quantified by the usual (quantum mechanical) dispersion. For the correlation function the variance is

$$\sigma^2(t) = \langle :\Phi^*(t)::\Phi(0)::\Phi^*(0)::\Phi(t):\rangle - C^2(t). \quad (3.8)$$

In quantum field theory, $\sigma^2(t)$ can be ultraviolet divergent, due to the composite operator $| : \Phi(0) : |^2$. Assuming t large enough for clustering, the divergence is

$$\sigma^2(t) \sim \langle | :\Phi(0): |^2\rangle^2 = C^2(0) \qquad (3.9)$$

—the statistical errors are proportional to $C(0)$! Thus the signal-to-noise ratio is

$$\frac{\text{SIGNAL}}{\text{NOISE}} = \frac{C(t)}{C(0)}. \qquad (3.10)$$

Eqs. (3.9) and (3.10) merely state the well-known fact that the absolute statistical errors are approximately t-independent, i.e. the relative statistical errors grow with t. Conversely, the *systematic* errors are greatest for smaller t, cf. eqs. (3.3) and (3.5).

3.3. Estimating the signal-to-noise ratio

To compromise between the systematic and statistical errors, a useful criterion is to maximize the signal-to-noise ratio at $t \gtrsim m^{-1} \gg a$. This can be done by selecting Φ_r intelligently. A versatile choice of Φ_r will have some variational parameters, which can be tuned for optimization. In order to be confident that eq. (3.5) is adequate, one wants to follow the signal at least to $t \gtrsim m^{-1}$. Otherwise, it is possible that an insidious combination of excited states and nonzero Θ effects has mimicked the shape of eq. (3.5).

To lowest order in perturbation theory the correlation function can be depicted as in fig. 3. It is unwise and unnecessary to treat the long-distance part of the gluonic time-evolution perturbatively. That part will be represented by a kernel defined by

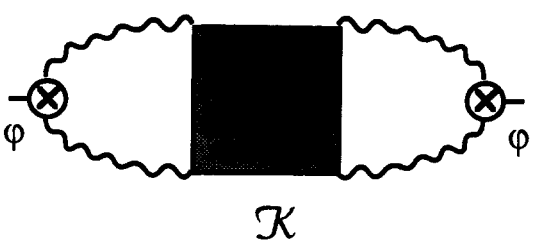

Figure 3: Diagrammatic expression for $C_r(t)$.

$$\langle :A(\tfrac{1}{2}P+k)A(\tfrac{1}{2}P-k)::A(\tfrac{1}{2}P'+k')A(\tfrac{1}{2}P'-k'):\rangle = (2\pi)^4\delta^{(4)}(P+P')\mathcal{K}(P|k,k'). \qquad (3.11)$$

(The following analysis suppresses the clutter of indices. The full analysis will appear elsewhere.[35]) In terms of $\mathcal{K}$ the correlation function is given by

$$C(t) = \int_{-\pi/a}^{\pi/a} \frac{dP_0}{2\pi}\frac{d^4k}{(2\pi)^4}\frac{d^4k'}{(2\pi)^4} e^{iP_0t} \times \varphi(P_0|k)\mathcal{K}(P_0|k,k')\varphi(P_0|k'), \qquad (3.12)$$

where φ arises from and depends on the choice of Φ. We are interested in the behaviour of this integral for $a \to 0$. The kernel $\mathcal{K}$ has length-dimension 8, which cancels the eight powers of momentum from the k and k' integration. For $t \neq 0$ the oscillatory factor permits us to complete the contour at $|P_0| = \pi/a$, and the P_0 integration then picks up contributions from the poles in the upper- (lower-) half-plane, for $t > 0$ ($t < 0$). For $t = 0$ there is no longer any damping at large $|P_0|$, and the integral diverges in the limit $a \to 0$; the degree of divergence depends on φ.

The "first generation" of glueball mass calculations employed small Wilson loops, such as the plaquette. This corresponds to $\varphi = [2\sin(\frac{1}{2}ka)/a]^2$, which has ultraviolet degree of divergence 2. The integral has two factors of φ and the diverging $\int dP_0$, whence

$$\frac{C(t)}{C(0)} \sim a^5. \qquad (3.13)$$

This behaviour is an obstacle to seeing continuum physics comparable to critical slowing-down. The problem is already apparent in the region $5.7 \leq \beta < 5.9$. Using data from a late "first generation" computation,[36] one finds the signal-to-noise ratio proportional to a^5, using the string tension to set the scale. The disastrous a^5 arises because local operators couple to long-distance

physics as $\varphi \approx k^2$. To improve on this, one must resort to nonlocal operators. Fortunately, there are (at least) four methods which are known to work. Let's see why.

3.4. Nonlocal operators

3.4.1. Adjoint lines

The first breakthrough came with the suggestion of using adjoint Polyakov loops (or Wilson lines).[13] A related method uses the product of two fundamental lines, displaced by a distance of order a. Here one has $\Phi = \mathrm{tr}[(\int_\Gamma A \cdot dx)^2]$, where the path Γ winds once around the torus. Consequently, φ does not introduce k^2 suppression in the infrared, and

$$\frac{C(t)}{C(0)} \sim a. \tag{3.14}$$

This method is straightforward to implement, and it has been very successful in small volumes. However, it seems plausible that this method will no longer outperform the others in the large z limit.

3.4.2. Fuzzy loops

Teper's fuzzing procedure[16] is inspired by the Monte Carlo renormalization group. In fact the first papers referred to it as "blocking," though the term "fuzzing" has now been adopted to avoid confusion. The procedure is depicted in fig. 4. The blocking is performed only in the spacelike directions, because unambiguous identification of the masses relies, through the transfer matrix, on operators with support on one timeslice; cf. sect. 2. In principle the α_i are tunable, though in practice it seems adequate to choose $\alpha_1 = \alpha_2$, such that the fuzzy link is in SU(N). A nice feature of this technique is that there are 2^3 times fewer fuzzy links than original links. Moreover, after iteration, a simple loop of very fuzzy links is a complicated linear combination of loops of original links. Consequently, elementary loops of fuzzy links are quite nonlocal when expressed in terms of the original links.

To see how fuzzing works, model it by

$$A_{\mathrm{fuzzy}} = \frac{1}{v_f} \int d^3x A(x) f(x), \tag{3.15}$$

with $v_f = \int d^3x f(x)$. Then the Fourier transform of the fuzzing-function f enters eq. (3.12), and if $f(k)$ falls off fast enough for large k, the integration converges (except perhaps $\int dP_0$) for all t and again one has

$$\frac{C(t)}{C(0)} \sim a, \tag{3.16}$$

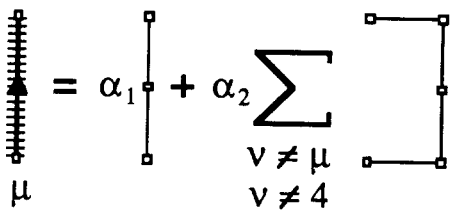

Figure 4: Depiction of Teper's algorithm for fuzzy links.

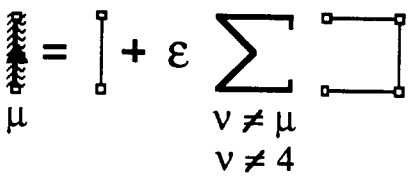

Figure 5: Depiction of Ape's algorithm for smearing.

as for the adjoint lines, but the reason is slightly different.

Of course, the fuzzing procedure, like most Monte Carlo renormalization group transformations, is just a recipe. Because of the complicated nonlinear nature of the system, it may turn out that the hypothesis of eq. (3.15) is too charitable, and that eq. (3.16) is too optimistic. Still, this method has provided the bulk of the numerical results covered in this review, so it obviously works very well at current values of β.

3.4.3. Smeared loops

The Ape collaboration's smearing method[37,38] is depicted in fig. 5. At the pictorial level, it appears quite similar to fuzzing, but note that smearing involves no factor-of-two blocking. Again, the transformation involves only spacelike links, out of respect for the transfer matrix. The effect of smearing, in a continuum notation, is similar to a diffusion equation:[37]

$$A_i = D_j F_{ji}. \tag{3.17}$$

In momentum space (and neglecting subtleties of the gauge), n_{it} iterations of the smearing procedure corresponds to

$$A_i(k) \to e^{-\tau k^2} A_i(k), \tag{3.18}$$

where $\tau \propto n_{\mathrm{it}}\varepsilon$ is the total elapsed "smearing time." The smeared plaquette thus has

$$\varphi \sim k^2 e^{-\tau k^2} \tag{3.19}$$

and, if $\tau \sim m^{-2}$, the k and k' integrations are cut off, even for $t = 0$. This is just a specific example of the trick discussed in sect. 3.4.2: smearing also suppresses the overlap with ultraviolet modes, and the signal-to-noise ratio is again

$$\frac{C(t)}{C(0)} \sim a. \tag{3.20}$$

This method has been very successful at $\beta = 5.9$.[37,38] Deeper into the continuum, the method will be critically slowed down: as $a \to 0$, with $\tau \sim m^{-2}$ fixed, one will find $n_{\rm it} \to \infty$.

3.4.4. Inverse Dirac operator

Like the adjoint line method, this method[39] breaks away from using local, albeit fuzzed or smeared, operators. Let $\mathcal{D}$ be a two- or three-dimensional staggered fermion matrix; then

$$\Phi = \sum_{\vec{x}} \mathrm{tr} \left(\frac{1}{\mathcal{D} + \mu} \right), \tag{3.21}$$

where μ is a variational parameter. The right-hand-side of eq. (3.21) is computed using Lanczos tridiagonalization.[39] To determine φ one has to examine a one-loop diagram over the (fictitious) staggered fermions.[35] One finds

$$\varphi(k) \approx 1 + O(k^2 a^2), \tag{3.22}$$

whence

$$\frac{C(t)}{C(0)} \sim a, \tag{3.23}$$

because the infrared suppression has been removed.

Note that this result does not depend on the dimensionality of the staggered fermions. Naively, one might expect that the two-dimensional operator wouldn't fare as well as the three-dimensional, because it is "thin" in one direction. However, the two-dimensional $\mathcal{D}$ is still nonlocal, and hence it evades the infrared suppression inherent in local operators. Initial results employing the two-dimensional Dirac operator indicate a^1 behaviour, using the string tension to set the scale.[39]

One selects specific glueball or electric-flux states by choosing various boundary conditions on $\mathcal{D}$ and constructing the combinations with appropriate $\mathbb{Z}_N^3$ quantum numbers. In the glueball sector, spin-parity is chosen by inserting a suitable γ-matrix inside the trace (for three-dimensional $\mathcal{D}$), or by taking appropriate combinations of planes (for two-dimensional $\mathcal{D}$).

The drawback of this method is that the Lanczos tridiagonalization becomes rather time-consuming for larger lattices, even for two-dimensional staggered fermions.

3.4.5. Which method is best?

In the absence of direct comparisons, this question is impossible to answer. It is likely that the methods mentioned above have different anomalous dimensions, although the computation would be rather tedious. Since no method is perfect, one option is to combine methods. For example, in small volumes fuzzy adjoint lines are an improvement over the usual adjoint lines.[40,41] Also, to reduce CPU-time refs. [38,39] have used one fuzzing step before smearing or tridiagonalizing $\mathcal{D}$ on their largest lattices.

4. RESULTS

The z-dependence of the SU(2) gauge theory has been thoroughly discussed in Part I. This part therefore concentrates on SU(3), except for occasional allusions to SU(2).

SU(3)'s analog of fig. 1 is in fig. 6; the Monte Carlo results[37,38,40,41,42,44,45,46] are qualitatively similar. Analytic work for SU(3) in intermediate volumes is in progress.[47] The numerical simulations have hence concentrated on large z, using the SU(2) simulations to indicate when z can be considered large. The error-bars in z are obtained directly from the original literature. The error-bars on the ratios are obtained by adding the errors of numerator and denominator in quadrature. This is not necessarily a reliable estimate; due to correlations in the data, the true (statistical) errors could be either smaller or larger.

For $z \lesssim 1.6$ vacuum-valley tunneling[48] can be neglected and the energy of electric flux essentially vanishes, making accurate Monte Carlo simulations extremely difficult. For $z \gtrsim 1.6$ the ratio $\sqrt{K}/m_{A_1^{++}}$ is only moderately z-dependent, but the qualitative trend is not what is expected from asymptotic formulae for K and m at large z.[30,31] However, fig. 6 has data from many different values of β, so a melange of finite lattice-spacing effects might throw up a smoke screen. Clearly, the asymptotic formulae can only be verified by fixing β (and hence a) and varying N_S. Nevertheless, the fact that several different groups agree, within error estimates, is significant and satisfying.

The situation for the E^{++} is somewhat less pleasing. In particular, the source method[37] does not agree

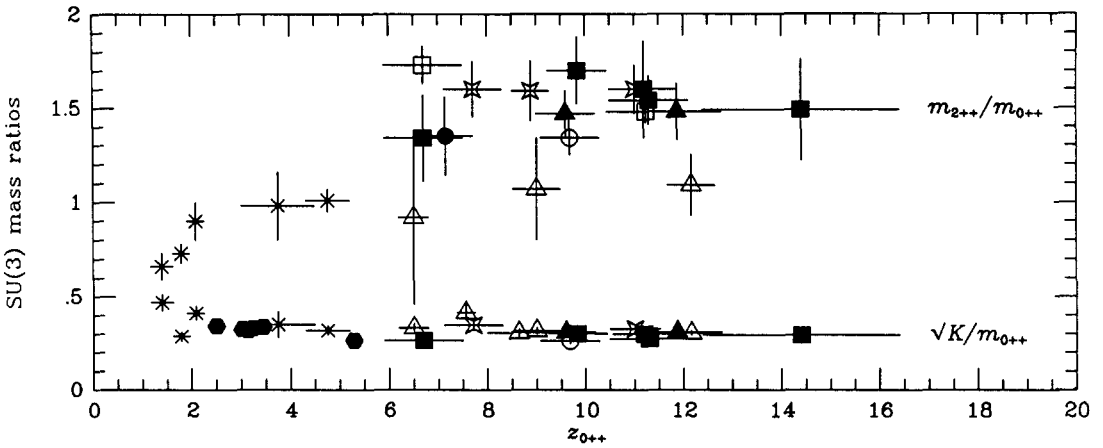

Figure 6: The SU(3) lattice Monte Carlo data for the mass ratios $\sqrt{K}/m_{A_1}$ (ordinates less than 0.5), m_E/m_{A_1} and m_{T_2}/m_{A_1} as a function of $z = z_{A_1}$ (ordinates greater than 0.5), all in the $PC = ++$ sector. Except for the crosses[42] and the solid circle[44] the data are since Seillac: open (T_2) and closed (K and E) squares,[40] open triangles,[37] closed triangles,[38] four-pointed stars,[45] hexagons,[41] and the open circle (which used a MCRG improved action).[46]

with the correlation method,[40,45] even from the same group.[38] It is tempting to blame the cold wall source and say that it does not couple well to the E representation. The error estimates for $m_{E^{++}}$ are large enough to raise eyebrows. Moreover, DeGrand's analysis[43] found very large (correctly normalized) χ^2 for the E state, in runs where the χ^2 was acceptable for K and $m_{A_1^{++}}$. However, the cold wall *does* couple well to the A_1^{++} and electric flux states, and the source method gives results for aE_1 and $am_{A_1^{++}}$ systematically lower than the correlation method. To explain this one must blame the negative coefficients in some terms of the expansion of eq. (3.7).

If one provisionally discards the source method results, one finds that the E^{++} and T_2^{++} states are degenerate for $z \gtrsim 7$, as in SU(2). Hence, it is sensible to compute the error-weighted averages over the $z \geq 7$ data contained in figs. 1 and 6. To reduce finite lattice-spacing effects, only data with $\beta \geq 2.3$ in SU(2) and $\beta \geq 5.9$ in SU(3) have been included. We find $\sqrt{K}/m_{A_1^{++}} = 0.308 \pm 0.020\,[0.265 \pm 0.016]$ and $m_{E^{++}}/m_{A_1^{++}} = 1.543 \pm 0.082\,[1.530 \pm 0.060]$ for SU(3) [SU(2)]. Given the agreement over several different simulations, it would be very surprising to see these numbers change in the pure glue theory. Of course, the inclusion of dynamical quarks could change the results, particularly through mixing; simulations along these lines are still at an embryonic state in their development.[49]

From a phenomenological point of view, numbers in MeV are most interesting. The best estimates presently available are collected in Table 3. The physical scale has been set by taking $\sqrt{K} = 420$ MeV. Scalar and tensor glueballs could be identified experimentally by finding additional states beyond (traditional) meson nonets. On the other hand, the 1^{-+} oddball has quantum numbers precluded by the quark model, so a state with those quantum numbers would be a clear glueball candidate. Unfortunately, the operators discussed in sect. 3 couple to this channel very weakly, too weakly even to as-

Table 3: Large z averages for the glueball masses in MeV, assuming $\sqrt{K} = 420$ MeV. For SU(2) there is no charge conjugation, so C should be ignored for the entries in the second column. See the note on the oddball in the text.

J^{PC}	SU(2)	SU(3)
0^{++}	1590 ± 100	1370 ± 90
2^{++}	2430 ± 100	2115 ± 125
1^{-+}		< 5000 ?% CL

sign a confidence level to the bound.[40] The techniques of sect. 3 will need some refinement, before definitive statements on these states are possible.

5. PROSPECTS

The status of the pure glue spectrum is very satisfactory. For $z \leq 5$ the agreement with the analytical methods is remarkable. The ratio $\sqrt{K}/m_{A_1^{++}}$ is in very good shape, $m_{E^{++}}/m_{A_1^{++}}$ and $m_{T_2^{++}}/m_{A_1^{++}}$ are in good shape, and we can hope that future simulations will have a handle on the oddballs. The numerical simulations can receive enough computer power so that the (estimates of) statistical errors are now comparable to (estimates of) systematic errors. Hence, a more thorough, more sophisticated error analysis[43,44] is now needed: the "systematic" effects of nonzero a and finite L can only be recognized and disentangled when the statistical errors are genuinely and reliably smaller. For example, the error bars are still too large to verify the prediction[31] for the ('t Hooft) string tension

$$K(L) = K(\infty) - \frac{\pi}{3L^2} \qquad (5.1)$$

based on the string picture. Finally, while the raw data (not shown here) do not yet exihibit asymptotic scaling, the tendency towards universal scaling is encouraging.

This status should be compared to 1985—the Wuppertal proceedings[50] contain no report on glueballs. In 1986 Berg, Billoire and Vohwinkel[14] had the first results in the scaling region, with the shocking result that m_E/m_{A_1} was slightly less than unity. While these results were correct, skeptics claimed that z was not yet large enough to draw conclusions for infinite z. It turns out that the skeptics were right, but it is unlikely that they really anticipated the dramatic changes in the masses that we see (somewhere) between 5 and 8. The region $5 < z < 10$ remains a puzzle. Its solution is motivation to go back to smaller lattices, for a change. At present the only clue is that $z = 7$ corresponds to 1 fm, which is exactly where things *should* happen.

ACKNOWLEDGEMENTS

One of us (PvB) thanks Fermilab for its hospitality during the preparation of the review. He is grateful to Jaap Hoek, Chris Korthals-Altes, Chris Michael, Mike Teper and Claus Vohwinkel for discussions and correspondence on the subject of this review. The other (ASK) recalls pleasant discussions on glueballs with Frank Brandstaeter, Martin Lüscher, Paul Mackenzie, and Gerrit Schierholz. He also thanks Bernd Berg, Tom DeGrand, Andreas Gocksch, Enzo Marinari, and Chris Michael for sending copies of their papers. Both of us wonder what the lattice conferences would be like without discussions with the other participants and Toscani cigars from Pietro Rossi. Finally we thank the organizers for bringing us together to review this subject, especially in a year that has seen much exciting progress on both the Monte Carlo and analytic fronts.

REFERENCES

1. A.H. Billoire, et al, eds., Nucl. Phys. B(Proc. Suppl.)4 (1988)
2. C. Michael, G.A. Tickle and M.J. Teper, Phys. Lett. 207B (1988)313
3. J. Koller and P. van Baal, Phys. Rev. Lett. 58 (1987) 2511; Nucl. Phys. B302 (1988) 1; Nucl. Phys. B(Proc. Suppl.)4 (1988) 47
4. C. Vohwinkel, Phys. Lett. 213B (1988) 54; this volume
5. J. Kripfganz and C. Michael, Liverpool preprint, LTH 216, July 1988
6. B.A. Berg, C. Vohwinkel and C.P. Korthals-Altes, Phys. Lett. 209B (1988) 319;
   B.A. Berg, this volume
7. P. Stephenson and M. Teper, work in progress (M. Teper, private communication)
8. D. Daniel, A. Gonzalez-Arroyo, C. Korthals-Altes and B. Söderberg, private communication by C.P. Korthals-Altes, to appear;
   A. Gonzalez-Arroyo and C.P. Korthals-Altes, Tallahassee preprint FSU-SCRI-87-77, to be revised
9. M. Lüscher, Phys. Lett. 118B (1982) 391
10. G. 't Hooft, Nucl. Phys. B153 (1979) 141
11. A. Billoire, K. Decker and R. Henzi, Phys. Lett. 211B (1988) 124
12. C. Michael and M. Teper, preprint (Oxford 40/88; Liverpool LTH 214)
13. B.A. Berg and A.H. Billoire, Phys. Lett. 166B (1986) 203; (E) 185B (1987) 466
14. B.A. Berg, A.H. Billoire and C. Vohwinkel, Phys. Rev. Lett. 57 (1986) 400
15. B.A. Berg, Nucl. Phys. B(Proc. Suppl.)4 (1988) 6
16. M. Teper, Phys. Lett. 183B (1986) 345; 185B (1987) 121
17. B. Carpenter, C. Michael and M. Teper, Phys. Lett. 198B (1987) 511
18. C. Michael and M. Teper, Phys. Lett. 199B (1987) 95
19. P. van Baal, Lectures at 28th Cracow School, CERN preprint TH.5141/88, August 1988

20. M. Lüscher, Nucl. Phys. B219 (1983) 233; M. Lüscher and G. Münster, Nucl. Phys. B232 (1984) 445
21. B.A. Berg and A.H. Billoire, private communication; SCRI preprint, in preparation
22. B.A. Berg, Phys. Lett. 206B (1988) 97
23. J. Hoek, M. Teper and J. Waterhouse, Nucl. Phys. B288 (1987) 589; J. Hoek, this volume; M. Kremer, A.S. Kronfeld, M.L. Laursen, G. Schierholz, C. Schleiermacher and U.-J. Wiese, Nucl. Phys. B305[FS23] (1988) 109; M.L. Laursen, this volume
24. P. van Baal, to appear in the proceedings of the workshop: Frontiers of Nonperturbative Field Theory, held in Eger (Hungary), CERN preprint TH.5215/88, October 1988
25. J. Kripfganz and C. Michael, Phys. Lett. 209B (1988) 77; P. van Baal, Nucl. Phys. B307 (1988) 274
26. B.A. Berg, A.H. Billoire and C. Vohwinkel, Phys. Lett. 191B (1987) 157
27. A. Gonzalez-Arroyo and M. Okawa, Phys. Rev. D27 (1983) 2397
28. A. Coste, A. Gonzalez-Arroyo, C.P. Korthals-Altes, B. Söderberg and A. Tarancon, Nucl. Phys. B287 (1987) 569
29. T.H. Hansson, P. van Baal and I. Zahed, Nucl. Phys. B289 (1987) 628
30. M. Lüscher, in *Progress in Gauge Field Theory*, G. 't Hooft et al, eds., (Plenum, New York, 1984); Comm. Math. Phys. 104 (1986) 277
31. R.D. Pisarski and O. Alvarez, Phys. Rev. D26 (1982) 3735; Ph. de Forcrand, G. Schierholz, H. Schneider and M. Teper, Phys. Lett. 160B (1985) 137
32. J. Groeneveld, J. Jurkiewicz and C.P. Korthals-Altes, Phys. Scripta 23 (1981) 1022
33. P. van Baal, Twisted Boundary Conditions: ..., Thesis, Utrecht (July 1984)
34. C. Michael, J. Phys. G13 (1987) 1001
35. F. Brandstaeter, A.S. Kronfeld and G. Schierholz, HLRZ preprint HLRZ 10/88.
36. Ph. de Forcrand, G. Schierholz, H. Schneider and M. Teper, Phys. Lett. 152B (1985) 107
37. Ape Collaboration: M. Albanese, et al, Phys. Lett. 192B (1987) 163; 205B (1988) 535
38. Ape Collaboration: M. Albanese, et al, Phys. Lett. 197B (1987) 400; L.A. Fernandez and E. Marinari, Nucl. Phys. B295[FS21] (1988) 51; E. Marinari, private communication ($\beta = 6$, $L = 18$ results)
39. G. Schierholz, Nucl. Phys. B(Proc. Suppl.)4 (1988) 11; A.S. Kronfeld, K.J.M. Moriarty and G. Schierholz, to appear in Comput. Phys. Commun.
40. C. Michael and M. Teper, Phys. Lett. 206B (1988) 299; Liverpool preprint LTH 218
41. J. Hoek, private communication
42. B.A. Berg, SCRI preprint FSU-SCRI-86-89 (unpublished)
43. T.A. DeGrand, Phys. Rev. D36 (1987) 176
44. T.A. DeGrand, Phys. Rev. D36 (1987) 3522
45. F. Brandstaeter, A.S. Kronfeld and G. Schierholz, in preparation; G. Schierholz, this volume
46. A. Patel, private communication
47. C. Vohwinkel, private communication
48. P. van Baal and J. Koller, Phys. Rev. Lett. 57 (1986) 2783
49. R.V. Gavai, A. Gocksch and U.M. Heller, Phys. Lett. 190B (1987) 282; A. Gocksch and U.M. Heller, Phys. Rev. Lett. 60 (1988) 1809
50. *Lattice Gauge Theory—A Challenge to Large Scale Computing*, edited by B. Bunk, K.-H. Mütter and K. Schilling (Plenum, New York, 1986)